



Cite this: *Green Chem.*, 2019, **21**, 491


Received 25th October 2018,

Accepted 14th January 2019

DOI: 10.1039/c8gc03345e

[rsc.li/greenchem](http://rsc.li/greenchem)

## Utilizing deactivated catalysts from the nitric oxide removal process for the fabrication of metal oxide/carbon supercapacitors†

Jiseok Lim,<sup>a</sup> Jungho Hwang<sup>\*b</sup> and Jeong Hoon Byeon <sup>\*a</sup>

Satisfying the criteria regarding greenhouse gas (GHG) emission and economic feasibility for the production of electrochemical energy storage devices is a challenging issue in a wide range of applications because the production of such devices involves costly materials and environmentally hazardous processes and typically requires electricity generated by conventional power plants (which also emit GHGs). In this regard, we propose a strategy to utilize waste catalysts used to remove nitric oxide (NO; one of the major emissions from thermoelectric power plants) for the fabrication of supercapacitors (SCs). Specifically, copper-deposited activated carbon fibers (Cu/ACFs) from a semi-dry electroless deposition process were used as catalysts for the ammonia-free selective catalytic reduction (SCR) of NO. Even though continuous SCR operation deactivated the Cu/ACFs into copper-oxide-deposited ACFs (CuO<sub>x</sub>/ACFs) as waste catalysts, the resultant architecture is preferably available for both capacitive charge and non-capacitive charge storage. Thus, the as-received CuO<sub>x</sub>/ACF was combined with an electrolyte gel *via* mechanical spraying and subsequently incorporated into separating and contacting electrodes for the fabrication of all-solid-state SCs. The fabricated SCs demonstrated superior volumetric capacitance and cycling stability, supporting the feasibility of utilizing waste NO removal catalysts in electrochemical energy storage.

Even though increasing global energy generation requires alternative or mixed energy sources to reduce greenhouse gas (GHG) emissions, energy generation using fossil fuels (*i.e.*, coals, natural gases, and oils) still represents approximately 90% (70% in electricity) of global energy consumption.<sup>1</sup> Moreover, global electricity generation has been increasing steadily, reaching approximately 24 000 TWh y<sup>-1</sup> in 2014.<sup>2</sup> This energy circumstance has thus ignited intensive research and

development (R&D) in renewable energy generation and energy storage systems (ESSs).<sup>3,4</sup> Because of intermittence issues related to renewable energy sources, however, ensuring stable and reliable energy generation and load balance remains a challenge.<sup>1</sup> As a promising approach, electrochemical ESSs, such as lithium-based batteries and supercapacitors (SCs), have been investigated for storing or reserving energy (mainly electricity) from power plants and trains.<sup>5,6</sup>

Advanced materials and architectures for electrochemical energy storage devices have recently been intensively investigated for their state-of-the-art applications in electric vehicles and electronic devices.<sup>7,8</sup> Even though numerous R&D efforts have provided some commercial opportunities for newly developed energy storage devices,<sup>9–11</sup> pollutant emissions (including GHGs) and resource consumption in the production of the storage devices have also become concerns for their realization.<sup>12–14</sup> In particular, researchers have attempted to fabricate SC devices from biological and industrial wastes to satisfy criteria such as low cost and low pollutant emissions for commercialization.<sup>15–19</sup> Carbonaceous and metallic compounds extracted from the wastes were reconstructed and used as active electrodes for fabricating the devices. Even though waste-derived electrodes exhibited superior electrochemical performance in SC devices, the transformation of waste into active electrodes required batch-wise harsh processes and toxic chemicals, which is inconsistent with the principles of environmental friendliness. Moreover, the devices are only capable of energy storage, not generation, implying that efficiently preventing global climate changes by reducing the operation of GHG-emitting traditional power plants remains a challenge. Hence, the development of a complementary concept for achieving more practical utilization of waste for the fabrication of SCs with minimal use of resources and emission of pollutants, as well as for providing guidance for stakeholders in the industry and policy of energy generation and storage, is desired.

In this regard, the present study proposes a complementary concept that utilizes waste environmental catalysts from after-treatment in combustion-based power generation (Fig. 1) for

<sup>a</sup>School of Mechanical Engineering, Yeungnam University, Gyeongsan 38541, Republic of Korea. E-mail: [postjb@yu.ac.kr](mailto:postjb@yu.ac.kr)

<sup>b</sup>School of Mechanical Engineering, Yonsei University, Seoul 03722, Republic of Korea. E-mail: [hwangjh@yonsei.ac.kr](mailto:hwangjh@yonsei.ac.kr)

†Electronic supplementary information (ESI) available. See DOI: 10.1039/c8gc03345e

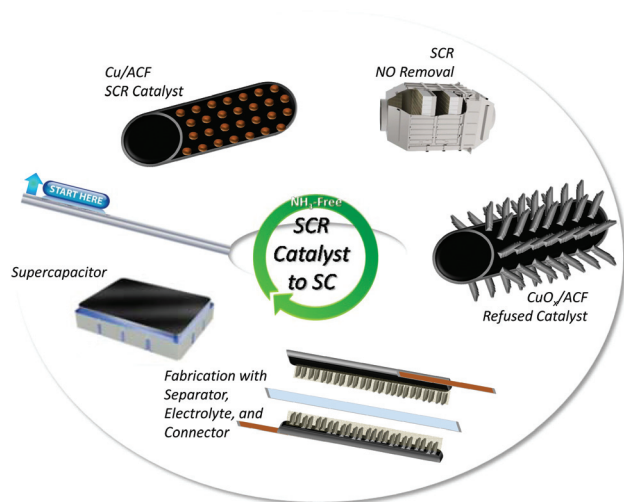


**Fig. 1** Utilization of refuse Cu/ACF catalysts (*i.e.*, CuO<sub>x</sub>/ACF) as active electrodes of SCs after they were used in the SCR of NO. The CuO<sub>x</sub>/ACF was utilized as received, along with separators, electrolytes, and connectors for the fabrication of SCs. This approach is proposed as a sustainable cycle for environmental catalysts for the efficient management of energy and resources in thermoelectric power plants.

the fabrication of electrochemical energy storage devices. Specifically, deactivated catalysts from the selective catalytic reduction (SCR) of nitric oxide (NO) were directly utilized with electrolytes, separators, and contacting electrodes for the fabrication of all-solid-state SCs. NO is one of the major pollutants in flue gases emitted from thermoelectric power plants (TPPs), and SCR with ammonia is usually used to remove the NO.<sup>20</sup> However, the ammonia supply for SCR leads to the undesirable formation of (NH<sub>4</sub>)<sub>2</sub>SO<sub>4</sub> or NH<sub>4</sub>HSO<sub>4</sub> because of ammonia slipping, causing the fouling of heat exchangers in TPPs; moreover, this SCR requires high temperatures (>350 °C) for effective operation.<sup>21</sup> To overcome this problem, researchers have replaced ammonia with carbon monoxide because it is less expensive and more readily available than ammonia.<sup>22,23</sup> Metal (chromium, iron, cobalt, nickel, and copper [Cu])/porous support composite catalysts exhibited greater activities than the metal catalyst or porous support alone in removing NO at low temperatures (<300 °C),<sup>24</sup> and the metal/activated carbon (AC) composite is also recognized as one of the effective configurations.<sup>25,26</sup> Deactivation of composite catalysts from constant SCR operation generally requires replacement or regeneration of the catalysts because of the growth of metal oxides (*i.e.*, less effective for SCR) on porous supports.<sup>27</sup> In the present study, we thus directly used deactivated catalysts (*e.g.*, Cu oxide/AC fibers [*i.e.*, CuO<sub>x</sub>/ACFs] in this study) from the NO removal process for fabricating SCs instead of replacing or regenerating them (Fig. S1, ESI†) because the ACF not only provides surfaces for high capacitance but also offers conductive paths for charge transfer.<sup>4,28,29</sup> Furthermore, CuO<sub>x</sub> has been recognized as a pseudocapacitive material; thus, a combination between CuO<sub>x</sub> and ACFs can demonstrate a synergy leading to superior electrochemical performance.<sup>30,31</sup> Similar

configurations (metal oxide on porous carbon) were also recently employed as high-performance capacitive materials for advanced SCs.<sup>32–34</sup> To this end, Cu-deposited ACFs (*i.e.*, Cu/ACFs) were first prepared *via* a semi-dry electroless Cu deposition. Atmospheric spark ablation between two silver (Ag) rods produced Ag nanoparticles (NPs) under negatively ionized (to prevent agglomeration between Ag NPs *via* repulsive forces) N<sub>2</sub> gas flow, and the Ag NPs were deposited onto ACF discs *via* mechanical filtration to catalytically activate the surfaces of the ACFs (Fig. S2, ESI†). The activated ACF discs were then immersed in an electroless Cu deposition bath to form Cu/ACF discs, which were subsequently rinsed with de-ionized water and dried under a particle-free atmosphere. The discs were packed into an SCR bed with graphite gaskets and fitted with cylindrical quartz tubes for NO removal tests (Fig. S3, ESI†). Finally, two deactivated discs were exposed to mechanical spraying of a polyvinyl alcohol (PVA)–H<sub>3</sub>PO<sub>4</sub> electrolyte and assembled with a glass-fiber membrane (separator) and two C foils (contacting electrodes) for the fabrication of an all-solid-state SC device (Fig. S1, ESI†). The electrochemical properties of the SCs and physicochemical characteristics of the Cu/ and CuO<sub>x</sub>/ACFs were investigated to examine the feasibility of using deactivated catalysts from the NO removal process as active electrodes of SCs.

For the uniform deposition of Cu particles onto the ACFs, a semi-dry electroless deposition method was adopted in this study, where the surfaces of ACFs were catalytically activated with aerosol Ag NPs produced by atmospheric spark ablation for subsequent electroless Cu deposition. The surface activation using aerosol NPs not only induced uniform deposition of metal particles even on curved surfaces (*i.e.*, fibers) but also reduced the use of wet chemistries and toxic chemicals, as well as the generation of waste.<sup>35</sup> To enhance sustainability even for catalyst preparation, as shown in Fig. S2a (ESI†), the spark-produced Ag NPs were directly deposited onto the surfaces of an ACF disc *via* mechanical filtration with gaseous unipolar ions (to suppress tight agglomeration between primary Ag particles *via* repulsive forces). The resultant geometric mean diameter, geometric standard deviation, and total number concentration were 28.0 nm, 1.55, and 8.8 × 10<sup>6</sup> particles per cm<sup>3</sup>, respectively (Fig. S2b, ESI†), as measured using a scanning mobility particle sizer (SMPS; 3936, TSI, USA). The collection efficiency as a function of particle diameter was found to be ~94%, implying that most of the Ag NPs had been deposited onto the surfaces of the ACFs. The morphology and microstructure of the Ag NPs observed by transmission electron microscopy (TEM; Tecnai G<sup>2</sup> F20 S-TWIN, FEI, USA) after direct aerosol sampling (*i.e.*, particle impaction on a carbon-coated Cu grid) were spherical and face-centered cubic (111) configurations, respectively (Fig. S2c, ESI†). The diameter of S particles in the TEM observation was ~3.7 nm, which was smaller than that (28.0 nm) measured by SMPS. This discrepancy indicates that the Ag particles in SMPS were agglomerates of several primary Ag particles. These agglomerates were broken up as primary particles during impaction onto the grid because of unipolar ions that caused loose agglomeration

between the primary particles. This loose agglomeration induced the uniform deposition of Ag NPs onto the surfaces of ACFs, rendering them ready to catalytically initiate Cu deposition (Fig. S2d, ESI†).

After Cu deposition and subsequent washing and drying, Cu/ACF discs were installed in an SCR bed for NO removal tests. An NO-carbon monoxide mixture gas ( $N_2$  balance) was injected into the SCR bed, and the concentration of NO was continuously monitored in the absence and presence of Cu/ACF discs to estimate removal efficiencies as a function of operating time (Fig. S3, ESI†). The concentrations of NO and carbon monoxide were controlled using mass flow controllers and were respectively set to 500 and 1000 ppm on the basis of previously reported results.<sup>21,36</sup> The operating temperature for the SCR was set to 230 °C on the basis of the results of the temperature-programmed desorption (TPD) of NO from the Cu/ACF and the untreated ACF (Fig. S4a, ESI†) because the SCR activity is relevant to the TPD of NO from catalysts.<sup>23,37</sup> The selected temperature also satisfies the temperature range for low-temperature SCR processes, which are desirable.<sup>24,38</sup> The temperature-programmed reduction (TPR) profile exhibi-

ted three bands at around 280 °C, 360 °C, and 520 °C, which matched the reductions for  $Cu^{2+}$  to  $Cu^+$ ,  $CuO_x$  rod to aggregate, and  $Cu^+$  to  $Cu^0$ , respectively (Fig. S4b, ESI†).<sup>22</sup> The bands at around 150 °C (reaction between carbon monoxide and O [in  $CuO_x$ ]), 400 °C (reduction of  $CuO$  to  $Cu^0$ ) and 650 °C (reduction of  $Cu_2O$  to  $Cu^0$ ) in the carbon monoxide-TPR profile (Fig. S4c, ESI†) further supported the reduction of  $CuO_x$  to  $Cu^0$ .<sup>39</sup> The residence time of NO-carbon monoxide in the SCR bed was selected as 1.8 and 3.6 s (4000 and 2000  $h^{-1}$  in gas hourly space velocity [GHSV]) to enable rapid analysis of the properties of the catalysts (*i.e.*, accelerating deactivation), and the catalysts at the early (Cu/ACF), middle ( $CuO_x$ -m/ACF), and closing ( $CuO_x$ -c/ACF) stages were characterized to confirm deactivation from the constant SCR operation.

As shown in Fig. 2a, the prepared catalysts clearly exhibited catalytic activity toward NO removal and the residence time affected the catalytic efficiency. During 6 h of operation, the removal activity steadily decreased with increasing operating time, likely because of deactivation of the catalysts. The adsorption isotherms were recorded using a porosimeter (ASAP 2010, Micromeritics, USA; Fig. 2b) for the three stages,

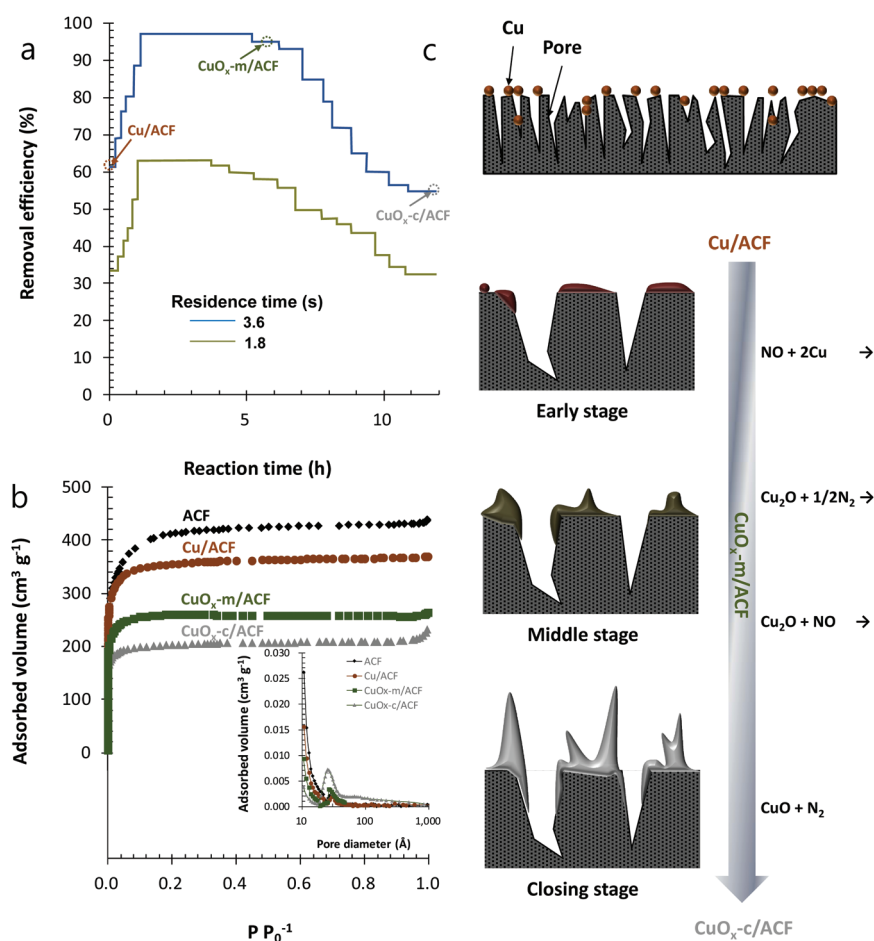
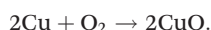
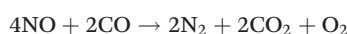


**Fig. 2** Formation of  $CuO_x$ /ACFs from NO removal. (a) Operating time-dependent profiles of NO removal using Cu/ACF catalysts for different NO residence times (1.8 and 3.6 s; 4000 and 2000  $h^{-1}$  in GHSV) at 250 °C gas temperature. (b) Changes in adsorbed volume and pore size distribution (inset) of Cu/ACFs after use in NO removal; the ACF is included for comparison. (c) Scheme for the formation of  $CuO_x$ /ACFs during NO removal. The  $O_2$  from NO reduction by Cu/ACFs caused the transformation of Cu into  $CuO_x$ .



including the untreated ACF to confirm the changes in textural properties. The pore volume of the untreated ACF was reduced upon Cu deposition (Cu/ACF), and it was further reduced when the operating time with the Cu/ACF installed for NO removal was increased. Interestingly, the fraction of the mesoporous region increased with increasing operating time (inset pore size distributions; Fig. 2b), whereas the microporosity decreased. This changed texture might enhance the electrochemical performance because mesopores (2–5 nm; might be originated from the voids between small CuO<sub>x</sub> particles after the SCR<sup>23</sup>) tend to improve capacitance and energy density for SC devices.<sup>28</sup> The decrease in microporosity is related to filling or blocking of the pores *via* the growth of mesoporous structures (*i.e.*, CuO<sub>x</sub>) on the surfaces of ACFs (Fig. 2c) because detached oxygen molecules from SCR can oxidize the surfaces of Cu particles *via* the following reactions:



The net reaction steps for copper(II) oxide growth from Cu during the constant NO removal process are also described in Fig. 2c.

The aforementioned hypothetical reactions regarding the deactivation of Cu/ACF catalysts were proven through the analysis of the morphologies and chemistries of the CuO<sub>x</sub>/ACF formed from the NO removal experiment. Fig. 3a shows low- and high-magnification scanning electron microscopy (SEM; JSM-6500F, JEOL, Japan) images of the Cu/ACF before it was used for NO removal. Spherical dots are densely distributed on the surfaces of the fibers, demonstrating that catalytic surface activation using Ag NPs is viable for achieving uniform Cu deposition on the fibrous structures. In the case of the CuO<sub>x</sub>-c/ACF (collected after 12 h of operation; Fig. 3b), hierarchical structures were grown on the surfaces of the fiber, supporting

the hypothesis of deactivation (Fig. 2c). Correspondingly, only Cu K signals were observed for the Cu/ACF (Fig. 3c) in elemental mapping analyses using energy-dispersive X-ray spectroscopy (EDX; JED-2300, JEOL, Japan), whereas significant O K signals (Fig. 3d) were observed after the catalyst was used to remove NO. Optical microscopy images further support the transformation of Cu/ACFs into CuO<sub>x</sub>/ACFs during NO removal by exhibiting different colors (Fig. 3e). X-ray diffraction (XRD; D/MAX-2500, Rigaku, Japan) patterns revealed characteristic peaks for Cu, CuO<sub>x</sub>-m, and CuO<sub>x</sub>-c on ACFs (Fig. 2f). An intense band assigned to the (111) plane of Cu was attenuated at the CuO<sub>x</sub>-m stage and then almost disappeared at the CuO<sub>x</sub>-c stage, whereas characteristic bands of CuO<sub>x</sub> were generated at both the CuO<sub>x</sub>-m and CuO<sub>x</sub>-c stages. The core level Cu 2p X-ray photoelectron spectroscopy (XPS; Axis-HIS, Kratos Analytical, Japan) profile of CuO<sub>x</sub>/ACFs exhibited satellite peaks associated with Cu<sup>2+</sup>, proving the formation of CuO<sub>x</sub> (Fig. S5, ESI†).<sup>40</sup> Specifically, the profile exhibited a Cu 2p<sub>3/2</sub> (or Cu 2p<sub>1/2</sub>) band at around 934 eV (or 953 eV) with a satellite band at around 944 eV (963 eV), which matched the fully oxidized CuO surface.<sup>41</sup> Thus, NO removal using Cu-supported catalysts is also a suitable gas-phase route to produce hierarchical CuO<sub>x</sub> structures on supports. In particular, the (110) band corresponding to CuO<sub>x</sub> was substantially intensified, possibly related to the growth of copper(II) oxide. This result was further verified by high-magnification TEM observations, which revealed a lattice fringe of 0.27 nm, which was assigned to the (110) plane of copper(II) oxide (Fig. S6, ESI†).<sup>42</sup> In addition, voids between the rod-like CuO<sub>x</sub> might cause the formation of macropores (inset of Fig. 2b, ESI†) after the SCR.

The CuO<sub>x</sub>-c/ACF was directly treated with mechanical spraying of a PVA–H<sub>3</sub>PO<sub>4</sub> electrolyte and dried to combine with a glass fiber disc (separating electrode) and Cu foils (contacting electrode) for the fabrication of an all-solid-state SC device. Cyclic voltammetry (CV; Fig. 4a) and galvanostatic charge–discharge (GCD, Fig. 4b) curves exhibited near-rectangular and

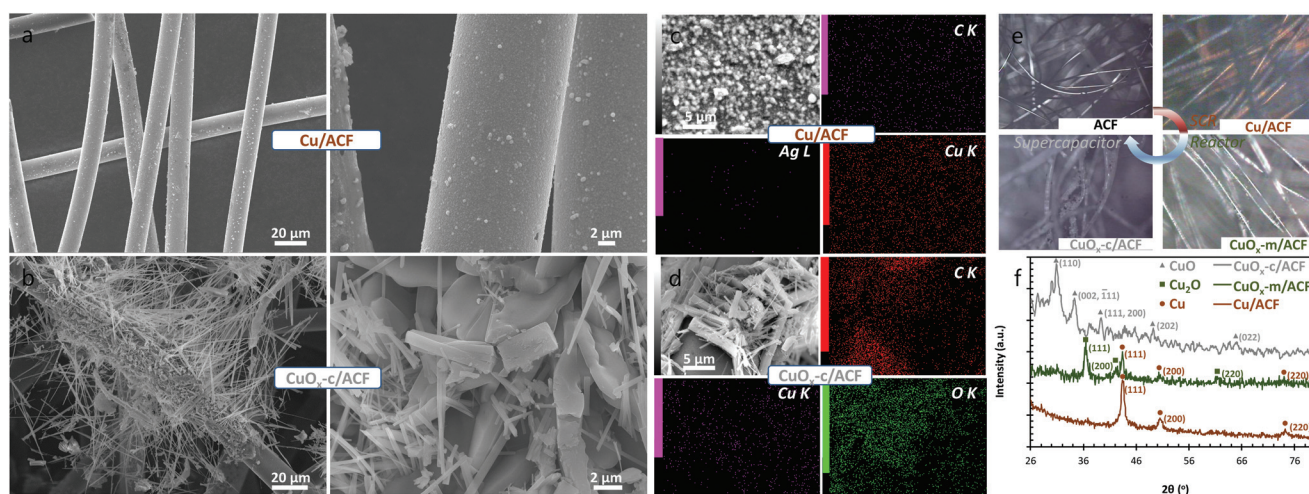
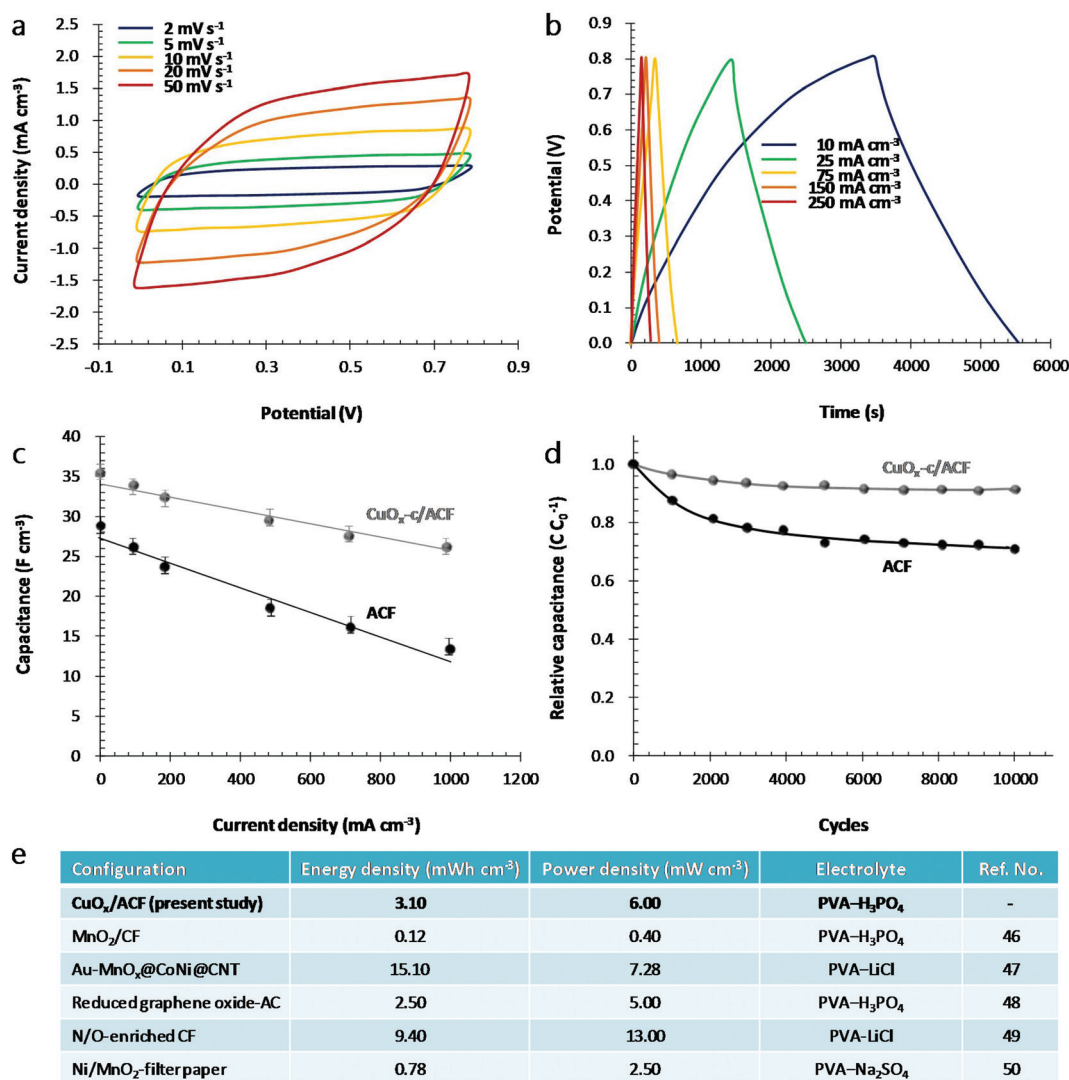


Fig. 3 Characterization of Cu/ and CuO<sub>x</sub>/ACFs: (a, b) low- and high-magnification SEM images; (c, d) elemental mapping images; (e) optical microscopy images; and (f) XRD patterns.



**Fig. 4** Electrochemical performance of CuO<sub>x</sub>-c/ACFs as active electrodes of all-solid-state SCs. (a, b) CV (recorded at different scan rates) and GCD (recorded at different current densities) curves. (c, d) Capacitance–current density and cycling stability (at 500 mA cm<sup>-2</sup>) profiles of CuO<sub>x</sub>-c/ACFs, including the ACF for comparison. (e) Energy and power densities of previously developed all-solid-state fibrous composite SCs for comparison with the present SC.

near-triangular shapes, respectively, representing good capacitive behavior of the fabricated device. No notable redox peaks in the CV curves can be found, which might be due to the single-sided formation of CuO<sub>x</sub> on ACFs after the SCR (most NO molecules adsorbed on one side of the Cu/ACF disc; refer to the reactor depicted in Fig. S3, ESI†). On the basis of the calculations from GCD curves, the device exhibited a mass capacitance of 74.7 F g<sup>-1</sup> at 10 mA cm<sup>-2</sup> and 64.4 F g<sup>-1</sup> at 250 mA cm<sup>-2</sup> (normalized to the two electrode volume). For this estimation, the electrode with a thickness of 200 μm and an active mass of 10 mg cm<sup>-2</sup> was fabricated referring to commercial electrodes.<sup>43</sup> The increasing rate of the voltage drop with increasing applied current density further suggests a comparable propagation of electric charges across the fabricated electrodes. The comparison in solid-state CV and GCD (Fig. S7a and S7b†) between CuO<sub>x</sub>-c-ACFs and ACFs (without CuO<sub>x</sub>)

further supports these results. Nevertheless, a distortion of the curves was identified, which might be caused by faradaic redox reactions of the nitrogen dopants originated from the SCR.<sup>44</sup> This suggests that further surface engineering, including structure tailoring arts might be required to secure a rational hierarchical structure for superior electrochemical performance. Even though the SC was fabricated with deactivated Cu/ACFs for NO removal, when the current density was increased, the SC with this deactivated material exhibited better rate capability than those fabricated from untreated clean ACFs (Fig. 4c). The three-electrode electrochemical test (Fig. S7c–S7e, ESI†) further supports the better capacity of the CuO<sub>x</sub>-c/ACF based SC than that of the ACF based SC. This result suggests that the increased fraction of mesoporosity introduced when Cu/ACFs were used for NO removal (*i.e.*, forming CuO<sub>x</sub>-c/ACFs) provided a suitable texture for efficient

access by electrolyte ions and for transport of the ions in the electrodes.<sup>45</sup> The stability of the SC during charge–discharge cycling also shows better performance than the SC fabricated from untreated ACFs, and the resulting capacitance was ~91% of its initial value after 10 000 cycles (Fig. 4d). This result further supports the feasibility of utilizing CuO<sub>x</sub>-c/ACFs to fabricate active electrodes of an SC device for introducing superior and stable capacitive activities. Fig. 4e summarizes the volumetric energy and power densities of recently developed all-solid-state fibrous composite SCs for comparison.<sup>46–50</sup> The densities of the fabricated SC in the present work is comparable with some of the previous reports, although fibrous SCs exhibiting greater performance are also introduced more recently.<sup>47,49</sup> Nevertheless, the present SC provides possibilities for the direct utilization of waste environmental catalysts; furthermore, the performance of the SC can be tuned through the use of different configurations of the catalyst (e.g., nickel/, cobalt/, ruthenium/, or manganese/ACF) for NO removal and different electrolytes in the fabrication of SCs using waste catalysts, as well as through applying posttreatments with better capacitive materials. Given the results observed for the present SC, the storage and delivery of electricity using this type of SC at TPPs as a complementary concept can also be expected to reduce TPP operation and conserve resources used in the manufacture of storage devices for energy and environmental sustainability; thus, this technology can be a stepping stone to effectively deal with the challenges facing global energy production and consumption.

## Conclusions

As a strategy model for achieving environmental sustainability, we used deactivated NO removal catalysts by directly incorporating them into PVA–H<sub>3</sub>PO<sub>4</sub> electrolytes to reduce undesirable pollutant emissions and resource consumption for the production of electrochemical energy storage devices. A semi-dry Cu deposition technique was used for the SCR of NO to ensure environmental friendliness even in the preparation of the Cu/ACF. Eventually, the as-received CuO<sub>x</sub>-c/ACFs (*i.e.*, deactivated catalyst) from the continuous SCR operation were treated by mechanical spraying of a PVA–H<sub>3</sub>PO<sub>4</sub> electrolyte and assembled with separating and contacting electrodes for the fabrication of all-solid-state SC devices. The resultant devices exhibited superior volumetric electrochemical capacitance and cycling stability. The concept proposed in this study not only provides a feasible strategy for the utilization of waste environmental catalysts for the fabrication of SCs but also offers conceptual insights into the complementary operation of traditional electric power plants and state-of-the-art energy storage devices for sustainable energy production and management.

## Conflicts of interest

There are no conflicts to declare.

## Acknowledgements

This work was supported by the National Research Foundation of Korea (NRF) Grant funded by the Korean Government (MSIP) (No. 2015R1A5A1037668).

## Notes and references

- 1 X. Luo, J. Wang, M. Dooner and J. Clarke, *Appl. Energy*, 2015, **137**, 511–536.
- 2 [https://en.wikipedia.org/wiki/World\\_energy\\_consumption](https://en.wikipedia.org/wiki/World_energy_consumption).
- 3 R. Patel, J. T. Park, M. Patel, J. K. Dash, E. B. Gowd, R. Karpoormath, A. Mishra, J. Kwak and J. H. Kim, *J. Mater. Chem. A*, 2018, **6**, 12–29.
- 4 H. Jiang, P. S. Lee and C. Li, *Energy Environ. Sci.*, 2013, **6**, 41–53.
- 5 C. Zou, L. Zhang, X. Hu, Z. Wang, T. Wik and M. Pecht, *J. Power Sources*, 2018, **390**, 286–296.
- 6 B. Zakeri and S. Syri, *Renewable Sustainable Energy Rev.*, 2015, **42**, 569–596.
- 7 Y. Fu, Q. Wei, G. Zhang and S. Sun, *Adv. Energy Mater.*, 2018, **8**, 1703058.
- 8 S. Niu, Z. Wang, M. Yu, M. Yu, L. Xiu, S. Wang, X. Wu and J. Qiu, *ACS Nano*, 2018, **12**, 3928–3937.
- 9 S. Panchal, M. Mathew, F. Fraser and M. Fowler, *Appl. Therm. Eng.*, 2018, **135**, 123–132.
- 10 M. Grützke, S. Krüger, V. Kraft, B. Vortmann, S. Rothermel, M. Winter and S. Nowak, *ChemSusChem*, 2015, **8**, 3433–3438.
- 11 C. Yang, Y. Tang, Y. Tian, Y. Luo, Y. He, X. Yin and W. Que, *Adv. Funct. Mater.*, 2018, **28**, 1705487.
- 12 Z. Chen, T. Yuan, X. Pu, H. Yang, X. Ai, Y. Xia and Y. Cao, *ACS Appl. Mater. Interfaces*, 2018, **10**, 11689–11698.
- 13 S. Yu, V. M. H. Ng, F. Wang, Z. Xiao, C. Li, L. B. Kong, W. Que and K. Zhou, *J. Mater. Chem. A*, 2018, **6**, 9332–9367.
- 14 H. Hao, Z. Mu, S. Jiang, Z. Liu and F. Zhao, *Sustainability*, 2017, **9**, 504.
- 15 W. Qian, F. Sun, Y. Xu, L. Qiu, C. Liu, S. Wang and F. Yan, *Energy Environ. Sci.*, 2014, **7**, 379–386.
- 16 S. T. Senthilkumar, N. Fu, Y. Liu, Y. Wang, L. Zhou and H. Huang, *Electrochim. Acta*, 2016, **211**, 411–419.
- 17 X. Duan, J. Deng, X. Wang, J. Guo and P. Liu, *J. Hazard. Mater.*, 2016, **312**, 319–328.
- 18 G. Nagaraju, S. C. Sekhar and J. S. Yu, *Adv. Energy Mater.*, 2018, **8**, 1700201.
- 19 C. Fu and P. S. Grant, *ACS Sustainable Chem. Eng.*, 2015, **3**, 2831–2838.
- 20 N. Yang, J.-l. Yu, J.-X. Dou, A. Tahmasebi, H. Song, B. Moghtaderi, J. Lucas and T. Wall, *Fuel Process. Technol.*, 2016, **152**, 102–107.
- 21 X. Cheng, Y. Cheng, Z. Wang and C. Ma, *Fuel*, 2018, **214**, 230–241.
- 22 A. Patel, P. Shukla, T. Rufford, S. Wang, J. Chen, V. Rudolph and Z. Zhu, *Appl. Catal., A*, 2011, **409–410**, 55–65.



- 23 I. Spassova, N. Stoeva, R. Nicklov, G. Atanasova and M. Khristova, *Appl. Surf. Sci.*, 2015, **369**, 120–129.
- 24 S. K. Papageorgiou, E. P. Favvas, A. A. Sapalidis and G. E. Romanos, *J. Hazard. Mater.*, 2011, **189**, 384–390.
- 25 B. Bhaduri and N. Verma, *J. Colloid Interface Sci.*, 2015, **457**, 62–71.
- 26 R. A. Catalão, F. J. Maldonado-Hódar, A. Fernandes, C. Henriques and M. F. Ribeiro, *Appl. Catal., B*, 2009, **88**, 135–141.
- 27 S.-J. Park and B.-J. Kim, *J. Colloid Interface Sci.*, 2005, **292**, 493–497.
- 28 Y. Huang, L. Peng, Y. Liu, G. Zhao, J. Y. Chen and G. Yu, *ACS Appl. Mater. Interfaces*, 2016, **8**, 15205–15215.
- 29 H. Wang, J. Deng, C. Xu, Y. Chen, F. Xu, J. Wang and Y. Wang, *Energy Storage Mater.*, 2017, **7**, 216–221.
- 30 W. Xu, S. Dai, G. Liu, Y. Xi, C. Hu and X. Wang, *Electrochim. Acta*, 2016, **203**, 1–8.
- 31 B. K. Deka, A. Hazarika, J. Kim, Y.-B. Park and H. W. Park, *Composites, Part A*, 2016, **87**, 256–262.
- 32 J. Chen, H. Wang, J. Deng, C. Xu and Y. Wang, *J. Mater. Chem. A*, 2018, **6**, 8986–8991.
- 33 H. Wang, R. Fan, J. Miao, J. Chen, S. Mao, J. Deng and Y. Wang, *J. Mater. Chem. A*, 2018, **6**, 6780–6784.
- 34 H. Wang, C. Xu, Y. Chen and Y. Wang, *Energy Storage Mater.*, 2017, **8**, 127–133.
- 35 J. H. Byeon, B. J. Ko and J. Hwang, *J. Phys. Chem. C*, 2008, **112**, 3627–3632.
- 36 R. W. Gerstle, S. T. Cuffe, A. A. Orning and C. H. Schwartz, *J. Air Pollut. Control Assoc.*, 1965, **15**, 59–64.
- 37 Y. Xue, Y. Guo, Z. Zhang, Y. Guo, Y. Wang and G. Lu, *Appl. Surf. Sci.*, 2008, **255**, 2591–2595.
- 38 M. Fu, C. Li, P. Lu, L. Qu, M. Zhang, Y. Zhou, M. Yu and Y. Fang, *Catal. Sci. Technol.*, 2014, **4**, 14–25.
- 39 H. Wang, K. Cai, J. Liu, X. Zhang, Y. Li, K. Cheng, J. Liu, C. Li, F. Ding and Y. Song, *RSC Adv.*, 2016, **6**, 84294–84308.
- 40 C.-K. Wu, M. Yin, S. O'Brien and J. T. Koberstein, *Chem. Mater.*, 2006, **18**, 6054–6058.
- 41 S. Poulston, P. M. Parlett, P. Stone and M. Bowker, *Surf. Interface Anal.*, 1996, **24**, 811–820.
- 42 Z. Li, Y. Chen, Y. Xin and Z. Zhang, *Sci. Rep.*, 2015, **5**, 16115.
- 43 M. Vijayakumar, R. Santhosh, J. Adduru, T. N. Rao and M. Karthik, *Carbon*, 2018, **140**, 465–476.
- 44 J. Zhou, J. Lian, L. Hou, J. Zhang, H. Gou, M. Xia, Y. Zhao, T. A. Strobel, L. Tao and F. Gao, *Nat. Commun.*, 2015, **6**, 8503.
- 45 L. Yuan, X.-H. Lu, X. Xiao, T. Zhai, J. Dai, F. Zhang, B. Hu, X. Wang, L. Gong, J. Chen, C. Hu, Y. Tong, J. Zhou and Z. L. Wang, *ACS Nano*, 2012, **6**, 656–661.
- 46 X. Xiao, T. Li, P. Yang, Y. Gao, H. Jin, W. Ni, W. Zhan, X. Zhang, Y. Cao, J. Zhong, L. Gong, W.-C. Yen, W. Mai, J. Chen, K. Huo, Y.-L. Chueh, Z. L. Wang and J. Zhou, *ACS Nano*, 2012, **6**, 9200–9206.
- 47 Z. Pan, J. Zhong, Q. Zhang, J. Yang, Y. Qui, X. Ding, K. Nie, H. Yuan, K. Feng, X. Wang, G. Xu, W. Li, Y. Yao, Q. Li, M. Liu and Y. Zhang, *Adv. Energy Mater.*, 2018, **8**, 1702946.
- 48 W. Ma, S. Chen, S. Yang, W. Chen, W. Weng and M. Zhu, *ACS Appl. Mater. Interfaces*, 2016, **8**, 14622–14627.
- 49 T. Qin, S. Peng, J. Hao, Y. Wen, Z. Wang, X. Wang, D. Ye, J. Zhang, J. Hou and G. Cao, *Adv. Energy Mater.*, 2017, **7**, 1700409.
- 50 L. Zhang, P. Zhu, F. Zhou, W. Zeng, H. Su, G. Li, J. Gao, R. Sun and C.-P. Wong, *ACS Nano*, 2016, **10**, 1273–1282.